Journal of Power Sources 185 (2008) 759–764

Contents lists available at ScienceDirect

Journal of Power Sources

journal homepage: www.elsevier.com/locate/jpowsour

Characterization of warpage behaviour of Gd-doped ceria/NiO–yttria stabilized zirconia bi-layer samples for solid oxide fuel cell application

Jaemyung Chang[a], Olivier Guillon[b], Jürgen Rödel[b], Suk-Joong L. Kang[a,*]

[a] Department of Materials Science and Engineering, Korea Advanced Institute of Science and Technology, 373-1 Guseong-dong, Yuseong-gu, Daejeon 305-701, Republic of Korea
[b] Institute of Materials Science, Technische Universität, Darmstadt D-64287, Germany

ARTICLE INFO

Article history:
Received 13 May 2008
Received in revised form 30 June 2008
Accepted 7 July 2008
Available online 3 August 2008

Keywords:
Continuum mechanics
Co-firing
Warpage
Solid oxide fuel cell
Viscoelastic analysis
Anode-support

ABSTRACT

To predict the warpage behaviour of an anode-supported half-cell of a solid oxide fuel cell (SOFC), a viscoelastic analysis has been made for a system with Gd-doped ceria (GDC) and NiO–yttria stabilized zirconia (NiO–YSZ) bi-layers. The viscoelastic properties of each component at 1573 K are measured by discontinuous sinter forging (for GDC) and continuous sinter forging (for NiO–YSZ) techniques. Using the measured uniaxial viscosities and the viscous Poisson ratio, the warpage during the co-firing of a GDC/NiO–YSZ bi-layer is calculated for the continuum mechanical models of Cai et al. and Kanters et al. The warpage predicted by the two models, in particular that of Cai et al., is shown to be in good quantitative agreement with the experimental observation. This result demonstrates that the warpage of bi-layer samples during co-firing can be suitably predicted when the viscoelastic properties of each component are properly measured and estimated. The present investigation also provides a useful methodology for optimizing the design of planar asymmetric half-cells for the SOFC industry.

1. Introduction

A planar geometry of stacked components is widely chosen for use in solid oxide fuel cells (SOFCs) due to its high power density and low fabrication cost [1,2]. One of the critical issues in fabricating a planar anode-supported SOFC is the co-firing of the solid electrolyte and anode. During the co-firing of asymmetric bi-layers, sintering defects such as cracks, debonding and warpage often occur due to the different densification rates that exist among the components. In order to solve this problem, the sintering behaviour of each component has to be characterized [3–11]. Nevertheless, few continuum mechanical approaches have been attempted in an effort to understand the co-firing processes of SOFC components.

Another issue in the fabrication of planar anode-supported SOFCs is related to their operating temperature. As the operation temperature of the well-known zirconia-based electrolyte is too high (~1273 K) for continuous use for a long period of time, other electrolyte materials have been investigated [1]. Gd- or Sm-doped ceria is each considered to be a good candidate for low-temperature operating SOFCs on account of the high electrical conductivity of ~0.08 S cm^{-1} at 1073 K [12,13]. As an anode material, a NiO–yttria stabilized zirconia (denoted as NiO–YSZ) composite is commonly used because of its good mechanical strength and chemical stability at a low partial pressure of oxygen [1,14].

To determine the viscoelastic behaviour of a porous multi-layer body throughout a densification process, the viscoelastic properties of individual layers initially have to be measured. Scherer [3] suggested that viscoelastic properties such as the uniaxial viscosity and viscous Poisson ratio could be determined from a linear viscous constitutive relationship of the mechanical response of a porous body. The uniaxial viscosity and viscous Poisson ratio as a function of the porosity are obtained by means of continuous [4], cyclic [5] and discontinuous sinter forging techniques [6–8].

The purpose of the present investigation is to predict the warpage behaviour of electrolyte|anode bi-layer samples using the measured viscoelastic properties of the components in a continuum mechanical approach and to test the applicability of the prediction by observing the warpage behaviour of bi-layer samples. The viscoelastic properties of nano-sized Gd-doped ceria (GDC) and NiO–YSZ are measured by discontinuous and continuous sinter forging techniques, respectively, and the warpage behaviour of the GDC/NiO–YSZ bi-layers during co-firing is evaluated. The observed warpage of the bi-layers at 1573 K is compared with calculations using models proposed by Cai et al. [9] and Kanters et al. [15].

* Corresponding author. Tel.: +82 42 869 4113; fax: +82 42 869 8920.
E-mail address: sjkang@kaist.ac.kr (S.-J.L. Kang).

0378-7753/$ – see front matter © 2008 Elsevier B.V. All rights reserved.
doi:10.1016/j.jpowsour.2008.07.075

2. Theoretical background

In cylindrical coordinates, the axial and radial strain rates of a sintering body, $\dot{\varepsilon}_z$ and $\dot{\varepsilon}_r$, are expressed, respectively, as [3]:

$$\dot{\varepsilon}_z = \dot{\varepsilon}_f + E_p^{-1}\ [\sigma_z - \nu_p(\sigma_r + \sigma_\theta)] \quad (1)$$

and

$$\dot{\varepsilon}_r = \dot{\varepsilon}_f + E_p^{-1}[\sigma_r - \nu_p(\sigma_\theta + \sigma_z)] \quad (2)$$

Assuming that the hoop and radial stresses, σ_θ and σ_r, are negligible under uniaxial loading, the uniaxial viscosity, E_p is defined by:

$$E_p = \frac{\sigma_z}{\dot{\varepsilon}_z - \dot{\varepsilon}_f} \quad (3)$$

where σ_z is the applied stress and $\dot{\varepsilon}_f$ is the free strain rate. Under the same assumption, the viscous Poisson ratio, ν_p, is expressed as [3]:

$$\nu_p = \frac{\dot{\varepsilon}_r - \dot{\varepsilon}_f}{\dot{\varepsilon}_z - \dot{\varepsilon}_f} \quad (4)$$

A more reliable method for determining ν_p has been derived from the volumetric densification rate, $\dot{\varepsilon}_v$, under uniaxial loading [16]:

$$\dot{\varepsilon}_v = \dot{\varepsilon}_z + 2\dot{\varepsilon}_r = 3\dot{\varepsilon}_f + \frac{\sigma_z}{E_p}(1 - 2\nu_p) \quad (5)$$

Given E_p, the viscous Poisson ratio can be determined.

Warping of an asymmetric bi-layer is due to the difference in the shrinkage rate between the two layers, which results in mismatch stresses [9]. Different continuum mechanical models can be used to predict the camber, all based on Kirchhoff assumptions (normals remain straight, unstretched and normal) for a thin plate and neglecting edge effects. The radial strain of the laminate ε'_r can be defined as [15]:

$$\varepsilon'_r(z) = \varepsilon'_0 - zk' \quad (6)$$

where k is the laminate camber (inverse of the curvature radius) and ε'_0 is the strain for $z = 0$ (by convention laminate mid-plane). Combining equations describing strain rates, Eqs. (1) and (2), the stress along the laminate thickness is expressed as:

$$\sigma_r(z) = \frac{E_p(z)}{1 - \nu_p(z)}(\dot{\varepsilon}'_0 - z\dot{k}' - \dot{z}k' - \dot{\varepsilon}_f(z)) \quad (7)$$

By applying the force and torque equilibrium on the entire system (discretized in 500 sub-layers), the two unknowns, k' and ε'_0, are deduced. The radial and axial strain rates are computed from Eqs. (1) and (2) and from the density distribution along the thickness axis. Sintering parameters (E_p, ν_p and $\dot{\varepsilon}_f$) are then corrected with the new calculated density for the next calculation step.

By neglecting the term $\dot{z}k'$ in Eq. (7) and the built-in stress that affects densification, the model of Cai et al. [9] allows a more straightforward calculation. This is given by:

$$\dot{k} = \frac{d((t_1 + t_2)/r)}{dt} = \left[\frac{6(m-1)^2 mn}{m^4n^2 + 2mn(2m^2 + 3m + 2) + 1}\right]\Delta\dot{\varepsilon} \quad (8)$$

where $\dot{k}$ is the rate of the curvature change normalized to the total thickness, $\Delta\dot{\varepsilon}$ is the mismatch between the free strain rates of two layers, m is the layer thickness ratio, t_1 and t_2 are the thickness of the two layers, r is the curvature radius of the bi-layer, n is the viscosity ratio between the layers and is expressed as [9]:

$$n = \frac{E_{p1}}{1 - \nu_{p1}}\frac{1 - \nu_{p2}}{E_{p2}} \quad (9)$$

3. Experimental procedure

3.1. Sample preparation for viscous property measurement

3.1.1. Gd-doped ceria

Nanocrystalline Gd-doped ceria ($Ce_{0.9}Gd_{0.1}O_{2-\delta}$, denoted as GDC, Rhodia, Germany) powder was used. The average size of the powder, as measured by the BET method (Autosorb 3B, Quantachrome), was 32 nm. As this Gd-doped ceria powder is nano-sized with a high driving force for densification, the densification was mostly completed upon reaching the co-firing temperature of 1573 K. Thus, the viscoelastic properties were measured at lower temperatures and they were estimated at higher temperatures through the use of appropriate functions of density, grain size and activation energy. Using a 12 mm diameter stainless-steel die, cylindrical pellets were uniaxially dry-pressed at 100 MPa. After cold isostatic pressing at 350 MPa for 120 s, the green body density was $60.7 \pm 0.3\%$ of the theoretical value.

Cylindrical pellets of a height of 16 mm were employed in sinter forging experiments using high-resolution axial and radial lasers to measure the height and diameter of the samples [17]. Some pellets were freely sintered, whereas others were sintered up to a desired density at 1323, 1373 and 1423 K. They were then temporarily subjected to a constant load of either 50 or 100 N, corresponding to 0.6 and 1.2 MPa, respectively. This mechanical load was applied within a 5% increase of relative density. The heating and cooling rate was set at 30 K min^{-1}. The density of each sintered sample was determined by the Archimedes method. The microstructure was characterized on fractured surfaces. The grain size was measured by the lineal intercept method with a correction coefficient of 1.56 using LINCE software (ver. 2.31, Ceramics Group, TU Darmstadt). As the mean grain size obtained from a fractured surface is smaller than that measured on a plane section by ~7% [15], compensation was made when presenting the data. More than 150 grains were examined for each sample.

3.1.2. NiO–YSZ composite

NiO (Sumitomo, Japan) and YSZ (TZ-8Y, Tosoh, Japan) were used to prepare a composition of 40 vol.% of NiO and 60 vol.% of YSZ. The mixed powders were ball-milled in ethanol for 24 h using 5 mm diameter zirconia balls. Green bodies 12 mm in diameter and 20 mm in height were compacted using a stainless-steel die at 100 MPa and were then cold isostatically pressed at 175 MPa for 120 s. The green density of the NiO–YSZ composite was 52.3% of the theoretical value determined by the rule of mixture. The shaped pellets were freely sintered at 1573 K, and some of them were then continuously subjected to a constant load of 100 N, corresponding to ~1.2 MPa. As the continuous and discontinuous sinter forging techniques gave similar results for alumina samples with a relative density lower than 80% [18], a continuous sinter forging technique was adopted. This technique requires fewer specimens compared with a discontinuous sinter forging technique. The heating and cooling rate was set to 30 K min^{-1}. The density of each sintered specimen was determined by the Archimedes method.

3.2. Observation of warpage behaviour of a GDC/NiO–YSZ bi-layer

Bi-layers of GDC and NiO–YSZ composite were prepared by a screen-printing method. The NiO–YSZ composite powder was dry-pressed at 100 MPa for 5 min in a 3 mm × 30 mm rectangular stainless-steel mold and pre-sintered at 1273 K for 30 min to obtain a relative density of $52.3 \pm 0.2\%$. The ethanol-based slurry of GDC was then screen-printed on to the prepared substrate composites.

The bi-layer was sintered at 1573 K in a tubular furnace and its shape was photographed through a transparent window with a CCD

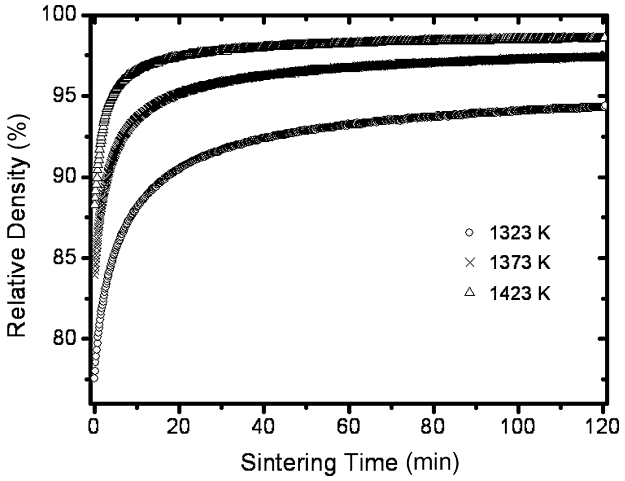

Fig. 1. Densification curves of GDC at three different temperatures.

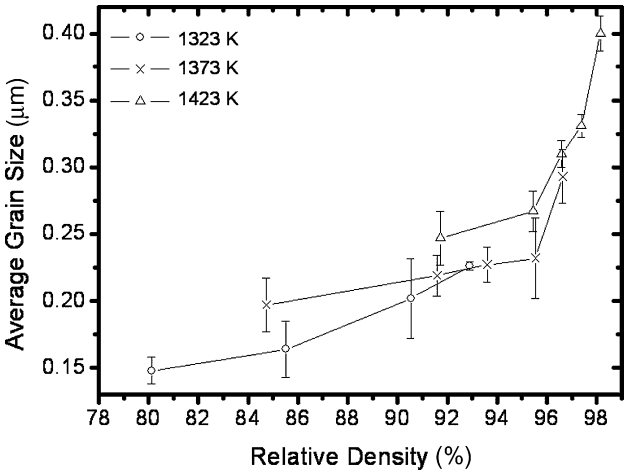

Fig. 3. Sintering trajectories of GDC at three different temperatures.

camera every 15 s. The heating rate was 30 K min^{-1}. The radii of a bi-layer were analyzed by an image analysis program (ImageJ, ver. 1.37, National Institute of Health). The thickness changes of the two layers with sintering time were measured by contact dilatometry (DIL 402C, Netzsch, Germany) using 1.0 mm × 1.0 mm square samples and identical heating schedules. (At the beginning of isothermal sintering, the thickness of the anode and the electrolyte were 1.8 mm and 24 μm, respectively.) With these small-size samples, it was possible to minimize the deflection due to the difference in the axial shrinkage between the two layers. The measured curvature was normalized to the measured thickness.

4. Results and discussion

4.1. Viscous properties of Gd-doped ceria

Densification curves of the GDC pellets are shown in Fig. 1. The sintering temperature could be reduced from the conventional sintering temperature of 1773–1973 to 1373 K using nano-sized GDC powder, as in the case of Li et al. [19]. The sintered density can be determined at any time by the following relationship:

$$\rho = \frac{\rho_0}{e^{(\varepsilon_z + 2\varepsilon_r)}} \tag{10}$$

Here, ρ_0 is the initial density and ε_z and ε_r are the true strains. The relative densities of the samples sintered at 1323, 1373 and 1423 K for 2 h were 94.5, 97.3 and 98.4%, respectively.

The uniaxial viscosity was determined from the linear relationship between the applied load and the axial strain rate. The overall uniaxial viscosities as a function of the relative density at three different temperatures are shown in Fig. 2. The uniaxial viscosity increases as the sintering proceeds and drastically increases when the specimen approaches its final density at each temperature. The drastic increase in the uniaxial viscosity is related to grain growth at the late stage of sintering [8].

The uniaxial viscosity can be expressed as independent functions of the grain size and relative density along with a thermally activated term [8,20,21]:

$$E_p = \alpha E_p(\rho) E_p(d)\, e^{(Q_d/kT)} \tag{11}$$

Here, α is a scaling factor, and $E_p(\rho)$ and $E_p(d)$ are functions of the relative density and grain size, respectively. For the same Gd-doped ceria, the function of density, $E_p(\rho)$, was previously found to follow Beere's model [8]. The function of the grain size, $E_p(d)$, is known to be proportional to the cube of the grain size normalized to the initial grain size for grain boundary diffusion [8,20,21], which is the case for this GDC. Fig. 3 plots the sintering trajectories of samples sintered freely at different temperatures. During the sintering process, the grain size increased from 150 to 400 nm.

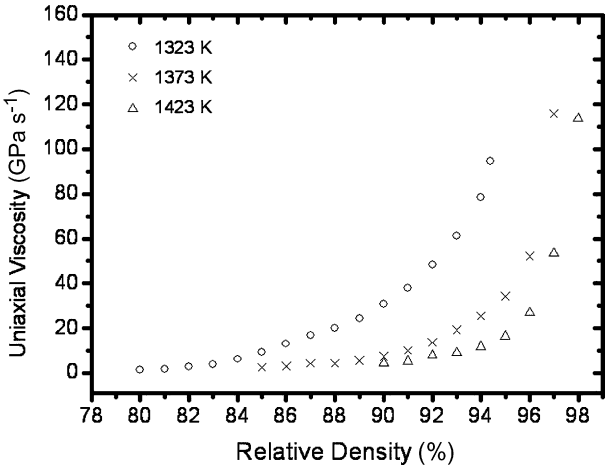

Fig. 2. Overall uniaxial viscosities with relative density of GDC at different temperatures.

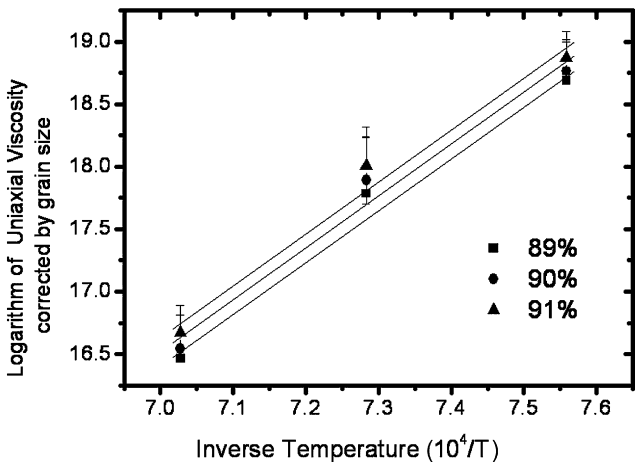

Fig. 4. Arrhenius plot of uniaxial viscosity normalized by grain size as function of inverse temperature.

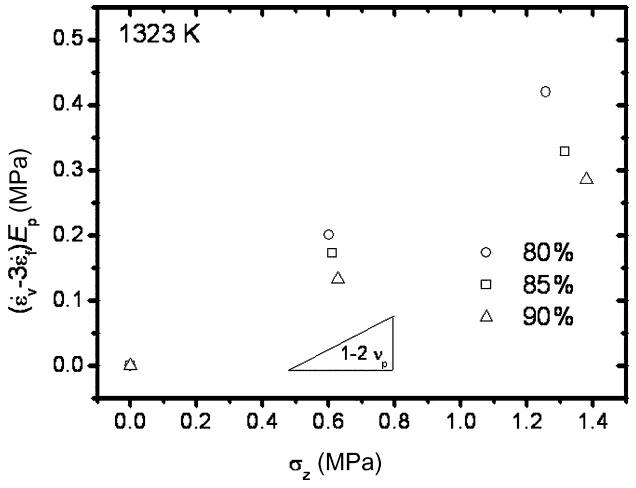

Fig. 5. Representative plot of volumetric densification rate as function of applied stress to determine viscous Poisson ratio at 1323 K.

The uniaxial viscosity normalized to the grain size was obtained using Eq. (11). This is given in Fig. 4 as a function of the inverse temperature. Its apparent activation energy is estimated to be 3.57 ± 0.05 eV from the slope of the Arrhenius plot.

The viscous Poisson ratio has also been determined by a discontinuous sinter forging technique. Fig. 5 shows a linear dependence between the applied stress and $(\dot{\varepsilon}_v - \dot{\varepsilon}_f)E_p$ at 80, 85 and 90% of the theoretical density at 1323 K. The slopes in the plots represent $1 - 2\nu_p$. The measured variation of the viscous Poisson ratio with the relative density at 1323 K is presented in Fig. 6. Each set of data points was obtained from a sample with a loading applied within a 5% increase of the relative density. For the range of 80–84% relative density, the measured values are in good agreement with the isotropic Venkatachari model, as has been observed for alumina compacts [22]. As the relative density increases above this range, the deviation from the model becomes larger. This may be due to the increased microstructural anisotropy induced by the uniaxial mechanical loading. A significant increase of the anisotropic viscous Poisson ratio ν_{31}^{p} has also been estimated by means of discrete element modelling for uniaxially loaded alumina compacts (direction 3 being the direction of the applied stress) [23].

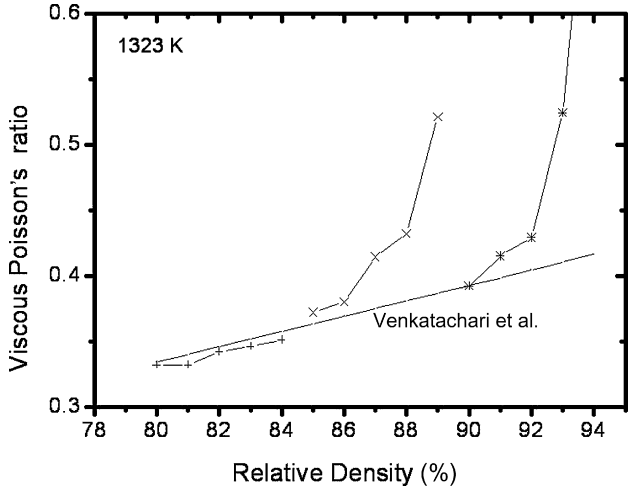

Fig. 6. Measured viscous Poisson ratio with relative density of GDC at 1323 K.

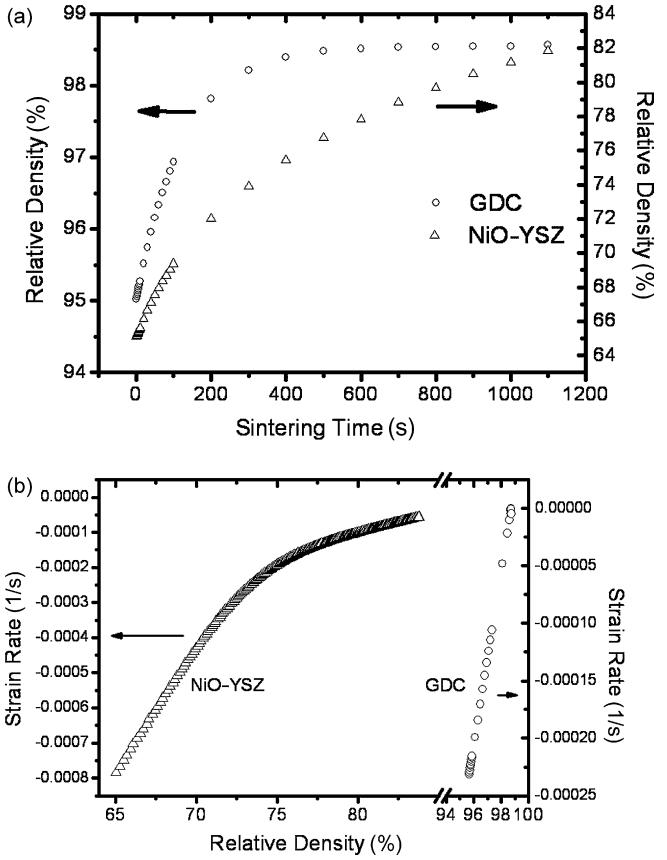

Fig. 7. Densification curves (a) and free strain rates (b) of GDC and NiO–YSZ composite at 1573 K.

4.2. Viscous properties of NiO–YSZ

Fig. 7(a) plots the free densification curves of NiO–YSZ (and GDC for comparison) at 1573 K as a function of the isothermal sintering time. Fig. 7(b) shows the free strain rate as a function of the density for 40NiO–60YSZ together with that for GDC at 1573 K. The free strain rate of NiO–YSZ is higher than that of GDC, as the relative density of the composite sintered at 1573 K for 30 min was only 82% of the theoretical value, whereas GDC becomes nearly fully densified after 200 s. The measured uniaxial viscosity of NiO–YSZ as a function of density is given in Fig. 8. The uniaxial viscosity of GDC

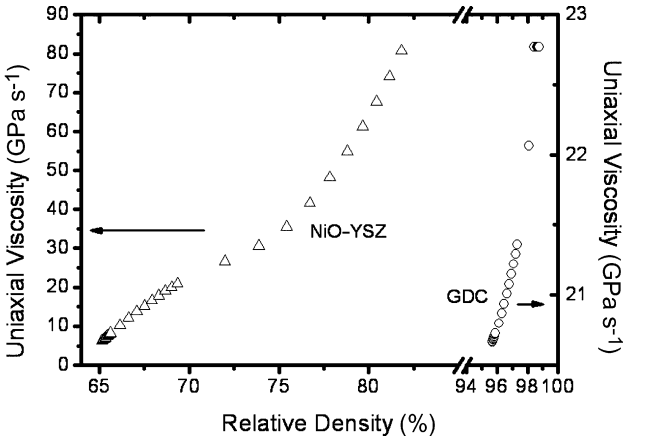

Fig. 8. Uniaxial viscosities of NiO–YSZ (measured) and GDC (estimated) as function of density at 1573 K.

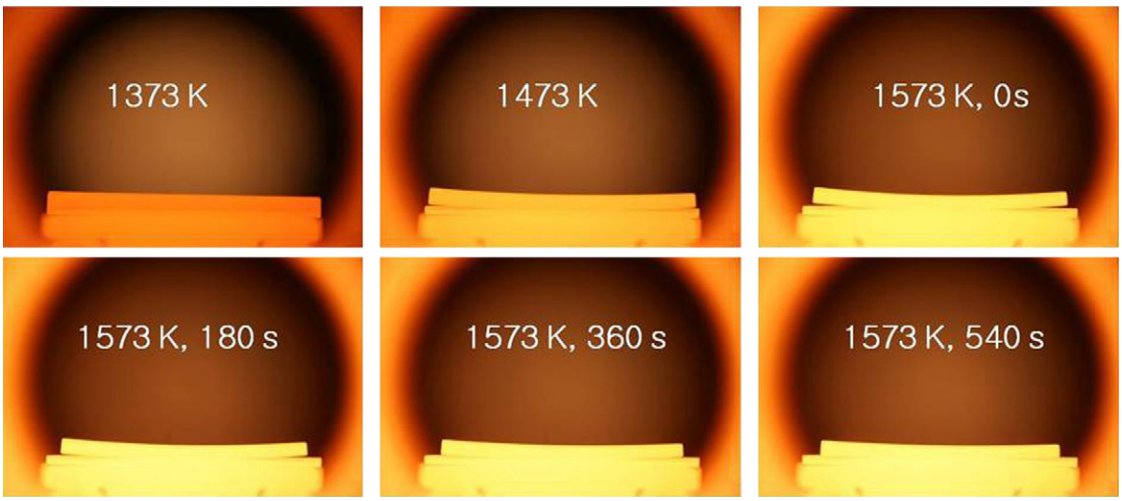

Fig. 9. Images of GDC/NiO–YSZ bi-layer during co-firing.

calculated using Eq. (11) is also plotted. The uniaxial viscosity value is nearly 80 GPa s^{-1} at 82% of the theoretical density. Given that the viscous Poisson ratio depends mainly on the relative density irrespective of the temperature and grain size [15,21], the Venkatachari model was also used to predict the sintering behaviour of the NiO–YSZ composite.

4.3. Evaluation of warpage behaviour of GDC/NiO–YSZ bi-layer

Images of warped bi-layers with a GDC layer on the top during co-firing are presented in Fig. 9. As the GDC layer sinters faster than the NiO–YSZ layer, the sample cambers upwards first. When the NiO–YSZ anode begins to sinter appreciably, the curvature decreases and eventually the sample flattens. Fig. 10 plots the variation of the curvature radius of a bi-layer sample while the sample is heated to 1573 K and upon isothermal holding at 1573 K. While it is heated to 1573 K, the radius decreases, i.e., sample warping increases. This level of warping is, however, very moderate compared with that observed in other systems, such as LTCC [24] and LSMZ/YSZ [25]. This is mainly due to the fact that the electrolyte GDC layer is very thin compared with the NiO–YSZ anode layer. For a thicker GDC layer, the large difference in the densification kinetics between the two materials should show a much higher curvature during sintering.

Fig. 11 plots the measured rate of the normalized curvature change as a function of the isothermal time at 1573 K. The predictions of warpage using the models of Cai et al. [9] and Kanters et al. [15] are also plotted in Fig. 11. An interesting aspect in this study is that the same experimental data were used for both models, allowing a direct comparison between the calculated curves. The measured and calculated rates are in good agreement. This result indicates that continuum mechanical models can be used to predict the warpage behaviour of a solid electrolyte|anode bi-layer if the viscous properties of the components are properly measured. The model of Cai et al. [9] insignificantly underestimates the camber rate for most of the time period, whereas the camber rate calculated using the model of Kanters et al. [15] is larger than the experimental value for the first 200 s of isothermal sintering. An apparently better agreement between the model of Cai et al. [9] and the measurement is observed in this study. Previously, Ravi and Green [10] measured viscoelastic properties by cyclic loading and calculated the warpage behaviour of laminated alumina tapes with different green densities. In their investigation, however, the agreement between the experimental and theoretical results during the isothermal sintering does not match that of this study. On the other hand, Kanters et al. [15] did not measure, but rather estimated, the viscous properties of zirconia layers using the theoretical model of Riedel et al. [26].

Fig. 10. Curvature radius of bi-layer measured during co-firing.

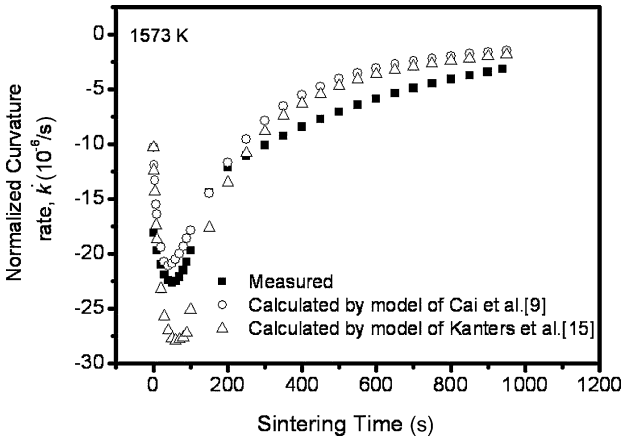

Fig. 11. Calculated and measured rate of normalized curvature change of bi-layer as function of time at 1573 K.

A number of reasons can be considered for the enhanced agreement in the present study, namely: (i) the discontinuous and continuous sinter forging techniques can be reliable for measuring the sintering parameters for high density and intermediate density regions, respectively, and (ii) the camber in the present system is much lower than usually observed in other systems, lowering the discrepancy between the model and the experiment. For identification of the main reason, however, further experiments with different geometries involving other systems are necessary.

The present investigation has shown that the warpage behaviour of an asymmetric half-cell of a solid electrolyte and an anode can be predicted well through the use of adequate continuum mechanics models when the viscoelastic properties of the materials are properly measured by discontinuous and continuous sinter forging with high precision. Once the sintering and viscoelastic properties are determined by a sinter forging technique, the critical design parameters of multi-layers can be optimized through iterative calculation (temperature program, thickness of the different layers and particle size of initial powder) to reduce undesired warpage. The methodology provided in the current work is also expected to be useful for evaluations and control of the warpage behaviour of other multi-layer structures and materials used in SOFC designs.

5. Conclusions

The viscoelastic properties of gadolium-doped ceria (GDC) and NiO–YSZ are determined via discontinuous and continuous sinter forging techniques to estimate the warpage behaviour of GDC|NiO–YSZ bi-layers. For the doped ceria, based on the grain size and temperature dependency of uniaxial viscosity, the uniaxial viscosity at 1573 K is estimated. The viscous Poisson ratio is determined by the linear relationship between the applied stress and the volumetric densification. The ratio estimated using the model of Venkatachari and Raj [20] is found to be in good agreement with the measured value. The uniaxial viscosity of the NiO–YSZ composite is determined using a continuous sinter forge technique at a temperature of 1573 K.

The warpage of bi-layers during sintering is directly observed in a furnace equipped with a CCD camera. During co-firing, the warpage of bi-layer samples with a thin electrolyte on a thick bulk anode is moderate; it increases at the beginning and decreases later. The warpage behaviour is also calculated through the use of the measured viscoelastic properties of the materials for two different models. The calculated results are in good quantitative agreement with the observation, in particular for that obtained using the model of Cai et al. [9]. It appears that the accuracy of constitutive parameters, in particular the viscous Poisson ratio, is critical for the prediction of warpage behaviour. The good agreement between the observed and predicted warpage in the present investigation demonstrates that the model calculation can successfully be applied for the optimization of the co-firing of bi-layer SOFC components when the viscous properties of the components are properly measured.

Acknowledgements

This work was supported by the project “Development of Core Technology for Intermediate Temperature Tubular SOFC Stack” funded by the Korean Government (MOCIE) and also by a Korea Research Foundation Grant funded by the Korean Government (MOEHRD) (KRF-2005-005-J09701). The authors thank Jean-Baptiste Ollagnier for his expertise in both mechanical models.

References

[1] M.Q. Minh, T. Takahashi, Science and Technology of Ceramic Fuel Cells, Elsevier, Amsterdam, 1995.
[2] P. Singh, N.Q. Minh, Int. J. Appl. Ceram. Technol. 1 (2004) 5–15.
[3] G.W. Scherer, J. Am. Ceram. Soc. 69 (1986) C206–C207.
[4] M.M.R. Boutz, L. Winnubst, A.J. Burggraaf, J. Am Ceram. Soc. 78 (1995) 121–128.
[5] P.Z. Cai, G.L. Messing, D.J. Green, J. Am. Ceram. Soc. 80 (1997) 445–452.
[6] R. Zuo, E. Aulbach, J. Rödel, Acta Mater. 51 (2003) 4563–4574.
[7] J.-B. Ollagnier, O. Guillon, J. Rödel, Int. J. Appl. Ceram. Technol. 3 (2006) 437–441.
[8] J. Chang, O. Guillon, J. Rödel, S.-J.L. Kang, Eur. Ceram. Soc. 27 (2007) 3127–3133.
[9] P.Z. Cai, D.J. Green, G.L. Messing, J. Am. Ceram. Soc. 80 (1997) 1929–1939.
[10] D. Ravi, D.J. Green, J. Eur. Ceram. Soc. 26 (2006) 17–25.
[11] D.J. Green, O. Guillon, J. Rödel, J. Eur. Ceram. Soc. 28 (2008) 1451–1466.
[12] J.B. Goodenough, Annu. Rev. Mater. Res. 33 (2003) 91–128.
[13] H. Inaba, H. Tagawa, Solid State Ionics 83 (1996) 1–16.
[14] H. Yokokawa, N. Sakai, T. Horita, K. Yamaji, Fuel Cells 1 (2001) 117–131.
[15] J. Kanters, U. Eisele, J. Rödel, J. Am. Ceram. Soc. 84 (2001) 2757–2763.
[16] J.-B. Ollagnier, O. Guillon, J. Rödel, J. Am. Ceram. Soc. 90 (2007) 3846–3851.
[17] E. Aulbach, R. Zuo, J. Rödel, Exp. Mech. 44 (2004) 71–75.
[18] R. Zuo, E. Aulbach, J. Rödel, Adv. Eng. Mater. 7 (2005) 949–952.
[19] J.-G. Li, T. Ikegami, T. Mori, Acta Mater. 52 (2004) 2221–2228.
[20] K.R. Venkatachari, R. Raj, J. Am. Ceram. Soc. 69 (1986) 499–506.
[21] R.K. Bordia, G.W. Scherer, Acta Metall. 36 (1988) 2399–2409.
[22] R. Zuo, E. Aulbach, J. Rödel, J. Mater. Res. 18 (2003) 2170–2176.
[23] A. Wonisch, O. Guillon, T. Kraft, M. Moseler, H. Riedel, J. Rödel, Acta Mater. 55 (2007) 5187–5199.
[24] R.T. Hsu, J.H. Jean, J. Am. Ceram. Soc. 88 (2005) 2429–2434.
[25] S.H. Lee, G.L. Messing, D.J. Green, Key Eng. Mater. 264–268 (2004) 321–328.
[26] H. Riedel, H. Zipse, J. Svoboda, Acta Metall. Mater. 42 (1994) 445–452.